Reinitialized versus Continuous Simulations for Regional Climate Downscaling

JIAN-HUA QIAN, ANJI SETH, AND STEPHEN ZEBIAK

International Research Institute for Climate Prediction, Columbia University, Palisades, New York

(Manuscript received 4 September 2002, in final form 2 June 2003)

ABSTRACT

The methodology for dynamical climate downscaling is studied using the second-generation regional climate model (RegCM2). The question addressed is, in order to simulate high-resolution details as accurately as possible, what strategy should be taken: continuous long-term integration in climate prediction mode or consecutive short-term integrations in weather forcasting mode? To investigate this problem, the model was run for 5 months in three different ways: 1) a 5-month continuous simulation, 2) monthly reinitialized simulations, and 3) 10-day reinitialized simulations. Compared to the observed precipitation, the 10-day reinitialized simulation results in the smallest error, while the continuous run shows larger error. Analysis shows that the long-term continuous simulation is contaminated by the systematic errors associated with the steep Andes Mountains and the uncertainties in the moisture processes in the planetary boundary layer near the coast. The method of 10-day reinitialization effectively mitigates the problem of systematic errors and makes a difference in the subtle precipitation processes in the regional climate model, therefore improving the accuracy in dynamic downscaling.

1. Introduction

Because of the constraint of computational resources, current climate prediction general circulation models (GCMs) typically use a horizontal grid size of about 200–500 km, which is too coarse for users in climate applications in hydrology, agriculture, and other areas. To obtain geographically more detailed information, either dynamic or statistical methods are used to downscale coarse-resolution reanalysis or GCM outputs to the high resolution needed over the area of application interests. Statistical downscaling employs empirical relationships between GCM outputs and local climate statistics (e.g., Wilby 1997). Dynamical downscaling requires a physically based high-resolution regional climate model driven by a coarse-resolution GCM or reanalysis to determine atmospheric and surface variables with the horizontal grid size between 20 and 100 km (Giorgi and Mearns 1999; McGregor 1997). This paper will only deal with the dynamic downscaling problem.

There is a distinction between regional climate downscaling and regional climate sensitivity studies. The purpose of downscaling is to obtain information in high-resolution detail as accurately as possible, whereas that of climate sensitivity experiments is to examine the anomaly response of the model to some internal or external forcings. Since the purposes of downscaling and sensitivity experiments are different, the optimal methodologies to address them might also be expected to differ. In sensitivity studies, a long-term simulation is needed in order to generate statistically significant differences between the test run and its control run, while the accuracy of spatial details may not be critically important. In contrast, in downscaling, the objective is to obtain high-resolution atmospheric and surface states (weather) and their statistics (climate) as close to reality as possible over the region of interest; therefore, the accuracy of the downscaling tool in reproducing regional structures and their temporal variability becomes critical.

Currently, the state-of-the-art atmospheric numerical models are still far from perfect, subject to internal error growth due to nonlinearity and instability and external (or systematic) error growth due to model deficiency (Lorenz 1963, 1969; Reynolds et al. 1994; Mo and Wang 1995; Pielke 1998). Unlike the fully autonomous global models, regional climate models are constrained by prescribed lateral boundary conditions. Because of this lateral control, the internal error growth is limited; hence, a so-called extended predictability (Anthes et al. 1985; Laprise et al. 2000) can be achieved for regional models. However, when a systematic error in some area persists or accumulates to a certain point, it contaminates other aspects of the model and degrades results elsewhere in the regional domain. Therefore, from the perspective of downscaling the problem is, how do we obtain optimal results based on currently available tools? A strategic question is whether the downscaling should be done by a sequence of short-term simulations in weather fore-

Corresponding author address: Dr. Jian-Hua (Joshua) Qian, International Research Institute for Climate Prediction, The Earth Institute at Columbia University, Lamont-Doherty Earth Observatory, P.O. Box 1000, 61 Route 9W, Palisades, NY 10964.
E-mail: jqian@iri.columbia.edu

casting mode or by a continuous long-term simulation in climate prediction mode. It is possible that the continuous long-term simulation, which is currently a common practice for both regional climate sensitivity study and regional climate downscaling, may not be the optimal method for downscaling. To mitigate the problem of systematic error accumulation in the continuous long-term simulations, the consecutive or periodically reinitialized short-term runs may provide better downscaling results. This paper is dedicated to studying this aspect of downscaling methodology.

In the original regional climate modeling study for the western United States, Dickinson et al. (1989) actually integrated an atmospheric mesoscale model version 4 (MM4) for a number of winter storms in a short-term weather forecasting mode. Later, the regional model was developed and applied in climate sensitivity studies with long-term integration (Giorgi and Bates 1989; Giorgi et al. 1993a,b; Giorgi and Marinucci 1996). In a study of the Asian summer monsoon, Ji and Vernekar (1997) ran a regional Eta Model nested within a GCM for a period of 1 month in two different ways: a 1-month continuous run and a reinitialized run by updating initial conditions every 48 h. They found that the reinitialized run was superior to the continuous run in both the intensity and spatial distribution of precipitation, mostly because of a model deficiency in the evaporation scheme over the ocean. Using a regional climate model (RegCM), the problem of reinitialization was investigated by Pan et al. (1999), who studied the long simulation of regional climate as a sequence of short segments (5-, 10-, or 30-day segments) for the U.S. Midwest Great Flood of 1993 in a 1-month period from 11 June to 11 July. For this midlatitude setting, it was found that for continuous integration without reinitialization, the location of maximum precipitation drifted downstream because simulated winds were too strong, implying the need for periodic reinitialization of the model. Druyan et al. (2001) used the Goddard Institute for Space Studies (GISS) regional climate model in a 2-week simulation of the West African wave turbulence and found that reinitialization on day 5 resulted in a dramatic improvement in the precipitation of the remaining 9 days, implying that information contained in the initial conditions was important for simulating rainfall. Based on the above examples of improved precipitation by short-term simulations, the problem of reinitialization is revisited in the current study in the context of regional climate downscaling, with the regional model setting over tropical South America, where the atmosphere is primarily driven by moist convection rather than baroclinic instability (Horel et al. 1994). A 5-month simulation (1 January–31 May 1985) also permits more comparisons among short (10-day), medium (monthly), and long (continuous) timescales.

Pan et al. (1999) also tested the effects of reinitializing soil moisture on precipitation in the Midwest region by comparing cases of periodically updated and continuously evolved soil moistures, as well as those of persistent moisture-saturated soil and persistent dry soil. Comparing the effect of changing soil moisture to that of updating atmospheric conditions, they found that the rainfall differences are small among those soil-moisture experiments, suggesting the secondary importance of soil-moisture memory for regional climate modeling in monthly timescales. Therefore, for simplicity, the present study concentrates on atmospheric processes only, and the effect of soil moisture is not examined.

A regional model can be driven by either reanalysis or GCM outputs. In the case of downscaling from reanalysis, the large-scale fields are assumed to be accurate, and the systematic errors are only associated with the deficiencies in the regional model. However, when a regional model is driven by a GCM, the driving large-scale fields are also subject to systematic errors from the global model. In this study, the regional model is driven by the National Centers for Environmental Prediction (NCEP)–National Center for Atmospheric Research (NCAR) reanalysis, focusing on the impact of error growth in the regional model on the accuracy of downscaling. The reinitialization experiment for downscaling driven by a GCM will be the topic of a separate study.

The numerical model and experimental design are described in section 2. In section 3, the continuous and reinitialized model simulations are compared to various observations in terms of monthly precipitation to examine their relative performances in downscaling. To understand the difference made by the reinitialized runs, the temporal evolution of the model variables are presented in section 4. In section 5. the spatial dependence of the domain interior to the lateral boundary forcing is examined. The systematic errors are analyzed in section 6. Section 7 gives the summary and discussion.

2. Model and experimental design

The numerical model used for this study is the second-generation regional climate model (RegCM2) developed by Giorgi et al. (1993a,b). It is also used by Seth and Rojas (2003) in a sensitivity study over South America. Its dynamical core is close to that of the hydrostatic version of the fifth-generation (Pennsylvania State University) PSU–NCAR Mesoscale Model (MM5), a gridpoint model (with an Arakawa B grid) based on primitive atmospheric equations. The vertical resolution is based on a pressure-based terrain-following σ coordinate,

$$\sigma = \frac{p - P_t}{P_s - P_t}, \tag{1}$$

where p is the air pressure in the atmosphere, P_s is the surface air pressure, and P_t is a prescribed constant pressure at the model top.

The regional model is driven by lateral boundary conditions provided by the NCEP–NCAR reanalysis. To

avoid discrepancies between the outer driving fields and the model internal physics, the exponential relaxation scheme of Giorgi et al. (1993b) is applied in the lateral buffer zone with a width of 14 grid intervals and consists of Newtonian and diffusion terms added to the model tendency equations for wind components, temperature, water vapor mixing ratio, and surface pressure. For a prognostic variable—for example, V—the nudging term is as follows:

$$\left(\frac{\partial V_M}{\partial t}\right)_n = F(n)F_1(V_{\rm LS} - V_M) - F(n)F_2\nabla^2(V_{\rm LS} - V_M), \quad (2)$$

where the subscripts LS and M refer to the driving large-scale and the model-simulated fields, respectively, and F_1 and F_2 are given by

$$F_1 = \frac{0.1}{\Delta t}, \qquad F_2 = \frac{\Delta x^2}{50\Delta t}, \quad (3)$$

where Δt and Δx are the model time step and horizontal grid size, respectively. The ∇^2 is the Laplace operator. The index n refers to the number of grid points from the lateral boundaries; that is, $n = 1$ on the outer boundary. The function $F(n)$ decreases from the outer boundary toward the inside of the buffer zone exponentially as

$$F(n) = \exp\left[-\frac{(n-2)}{N_I}\right], \qquad 2 \le n \le 14, \quad (4)$$

where the parameter N_I is used to adjust the extent of manipulation by the prescribed driving field in the buffer zone, with larger N_I the stronger control of the driving field. Larger N_I is used in the upper levels for stronger guidance of the driving large-scale circulation, but smaller N_I is used in the lower levels to let the regional model have more freedom to develop its own mesoscale features. The N_Is used in this study are (3, 3, 3, 3, 3, 2, 2, 2, 1, 1, 1, 1, 1, 1) for each σ level from top to bottom.

The regional model is totally governed by its own physics in the inner domain surrounded by the lateral buffer zone, only subject to the forcing by the underlying lower boundary of land and ocean. Over land area, the Biosphere–Atmosphere Transfer Scheme (BATS) (Dickinson et al. 1993) is employed to compute surface radiative, sensible, and latent heat, momentum fluxes, and surface temperature based on the assigned vegetation and soil parameters. Over the ocean, the model is forced by the sea surface temperature (SST) spatially and temporally interpolated from a monthly SST dataset. The resolvable scale precipitation is calculated by a simplified explicit moisture scheme described by Giorgi and Marinucci (1996), and the cloud water and fractional cover are used for cloud-radiation computations. The Grell (1993) cumulus scheme is used to calculate the precipitation due to moist convection. The parameterization scheme of the diabatic heating by solar and terrestrial radiation is that of the NCAR Community Climate Model Version 3 (CCM3) (Kiehl et al. 1996). Finally, the parameterizations representing subgrid-scale processes in the planetary boundary layer, such as turbulent transfer of momentum and heat in the lower atmosphere, are those of Holtslag et al. (1990).

Figure 1 shows the model domain (D1) that covers tropical and subtropical South America and the surrounding oceans, with an area of about 8000 × 6000 km^2. The model is run with a uniform grid of 60 km on a Mercator projection map. The area between D1 and D2 is the lateral relaxation buffer zone. Boxes D3 and D4 are only used later for diagnosis purposes. The model has 14 vertical levels, with 5 levels in the lowest 1.5 km of the atmosphere, and the top of the model atmosphere is at 80 hPa (P_t). The model was run from 1 January to 31 May 1985, with a time step of 3 min.

To examine the sensitivity of the regional model to initial conditions versus boundary conditions, three types of time integration were conducted. In the continuous run, the model was integrated from 0000 UTC 1 January 1985 to 0000 UTC 31 May 1985 without interuption for reinitializations (1 × 150 days). In the second simulation, the model was reinitialized every 30 days and it was called the monthly run for simplicity. Considering the initial shock (a dramatic fast adjustment caused by the imbalance between the coarse-resolution driving field and the high-resolution regional model dynamics and physics), the reinitializations are actually done at 2 days before the beginning of each 30-day segment (except for January; starting at 0000 UTC 1 January), and the outputs during the first 2 days of adjustment were excluded from the analysis data to ensure a fair comparison (5 × 32 days). For example, the second monthly run started at 0000 UTC 29 January with an integration period of 32 days, and only the outputs after 0000 UTC 31 January were used for analyses. In the 10-day run, the model was reinitialized every 10 days, with the outputs of the preceding 2 days excluded from the data analysis (15 × 12 days).

3. Comparison of simulated and observed precipitations

The continuous, monthly reinitialized, and 10-day reinitialized simulated precipitations were compared to three observational datasets: 1) the University of East Anglia (UEA) gridded monthly precipitation dataset (0.5°) based on station data from 1901–96 (New et al. 2000); 2) the Climate Prediction Center (CPC) Merged Analysis of Precipitation (CMAP), a blended monthly precipitation dataset (2.5° × 2.5° grid) using gauge and satellite observations and numerical model results (Xie and Arkin 1996, hereafter XA); and 3) the Brazil Agencia National de Energia Electria (ANEEL) daily precipitation data, available at the In-

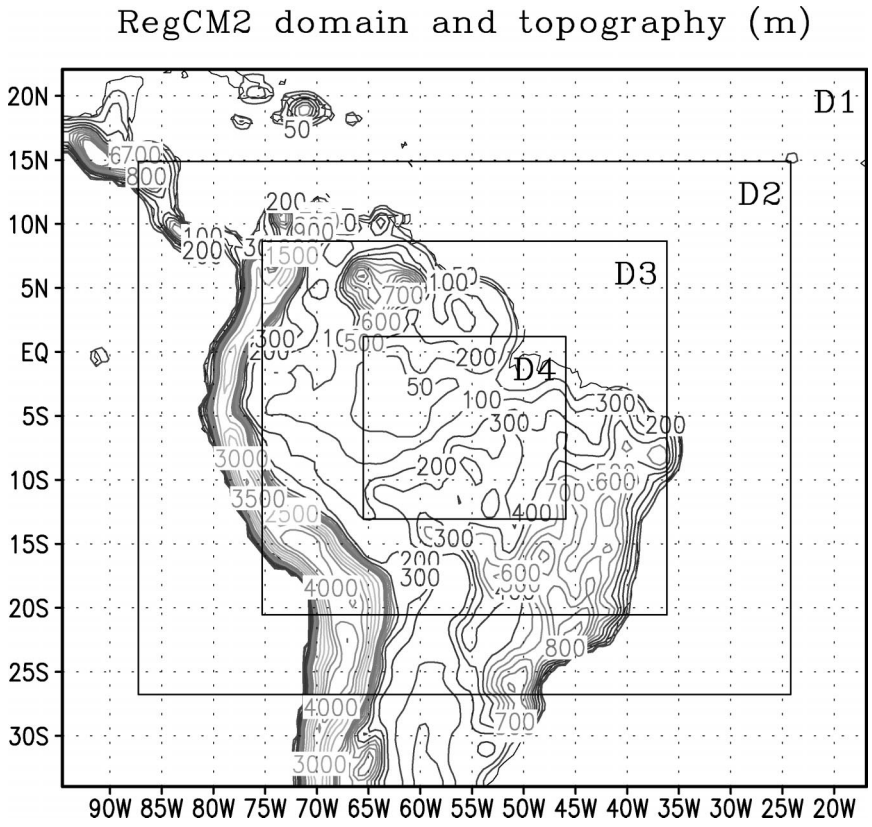

FIG. 1. Model domain (D1), buffer zone (between D1 and D2), diagnosis domains (D3 and D4), and topography (m).

ternational Research Institute for Climate Prediction (IRI). The ANEEL data are from meteorological stations along the Brazilian rivers and therefore only cover a limited area of the continental South America. This daily precipitation will be used for comparison in submonthly timescales.

Figure 2 shows the 5-month (January–May 1985) total precipitation of the three RegCM2 runs and that of UEA and XA. In the observational data, the maximum precipitation is over 1000 mm in the equatorial region from the Amazon River basin, to the Amazon mouth, and farther east to the equatorial Atlantic Ocean, corresponding to the Atlantic intertropical convergence zone (ITCZ). The secondary maximum extends from the Amazon basin to the southeast, corresponding to the South Atlantic convergence zone (SACZ). The precipitation minima are between the ITCZ and SACZ (about the area of the State of Bahia in Brazil) and over the North Atlantic and Pacific Oceans. The RegCM2 simulations reproduced both the ITCZ and SACZ precipitation maxima in roughly the correct locations, as well as the precipitation minima over the oceans. However, the precipitation in the Amazon basin is underestimated. Although the three model simulations are very similar, it is notable that the 10-day run produces the most precipitation in the Amazon basin and the least precipitation over the State of Bahia, thus the closest to the observations. The values in Fig. 2f show that the total Amazon rainfall (averaged in the rectangular box shown in Fig. 2a) is 991 mm in the 10-day reinitialized run, exceeding continuous and monthly runs by more than 100 mm, thus reducing the rainfall deficit with respect to the UEA and XA observations. In the SACZ region near the southeastern coast of Brazil, the continuous and monthly runs produce more precipitation than the 10-day run. The heavy precipitation belt along the eastern side of the Andes peak is presented in all three simulations, but it is not so strong in UEA and XA observational data; therefore, it seems to be the result of numerical errors in the treatment of the steep topography of the Andes.

To compare the seasonal variation, the area-averaged monthly precipitations over the Amazon basin, Nordeste (northeast Brazil), and southeast Brazil are shown in Fig. 3. Besides the UEA and XA monthly precipitations, the ANEEL daily data, averaged monthly and over the stations in the corresponding regions, are also shown. In Nordeste and Amazon, the ANEEL curve is quite different from those of UEA and XA, and the latter two are relatively close to each other, implying large uncertainties even in the observational or analysis fields. In the southeast region, however, the three observational

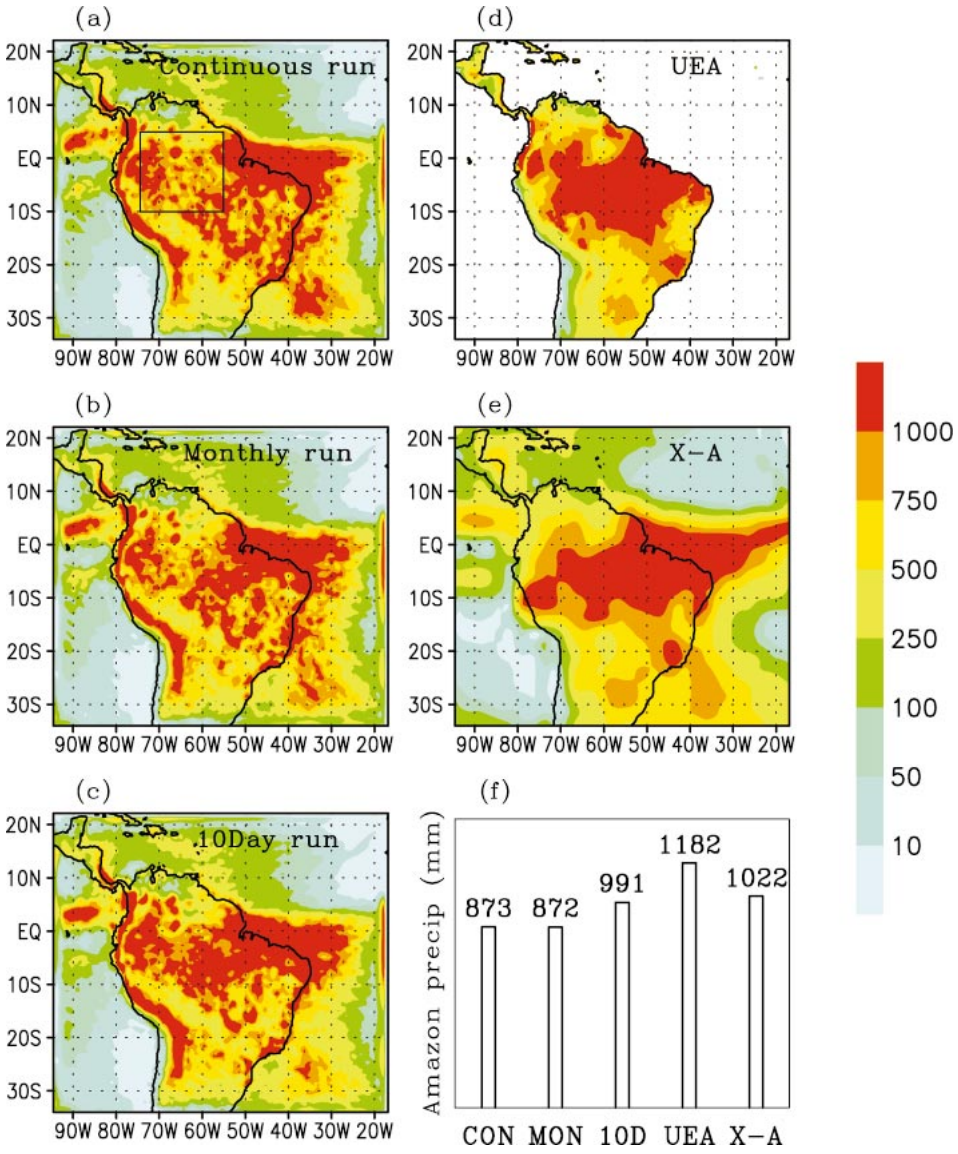

FIG. 2. Total precipitation (mm), Jan–May 1985: (a) RegCM2 continuous run, (b) RegCM2 monthly reinitialized run, (c) RegCM2 10-day reinitialized run, (d) University of East Anglia (UEA) 0.5° gridded observational data over land, (e) Xie–Arkin (X–A) blended gauge, satellite observations, and numerical model data, and (f) 5-month total precipitation (mm) averaged over the Amazon, from the boxed region in (a).

datasets are fairly close to each other. In Nordeste, the three simulations are close to each other, with the 10-day run results very close to the UEA data from Febuary to May. In the Amazon region, the precipitation in the 10-day run is the closest to the observations for every month. For the southeast region, the seasonal variational trend of continuous and monthly runs is better than that of 10-day run, although the difference with the observations is smaller in the 10-day run from Febuary to April. Further comparisons in submonthly scales will be described in the next section.

4. Temporal adjustment between the regional model and the driving field

a. Initial shock

To understand why the reinitialized runs produce better results, the evolution and adjustment of model variables from synoptic to monthly timescales are examined. Two stages of temporal adjustments are detected in the model spinup process: the initial sharp adjustment (initial shock) within the first 1 or 2 days and the sub-

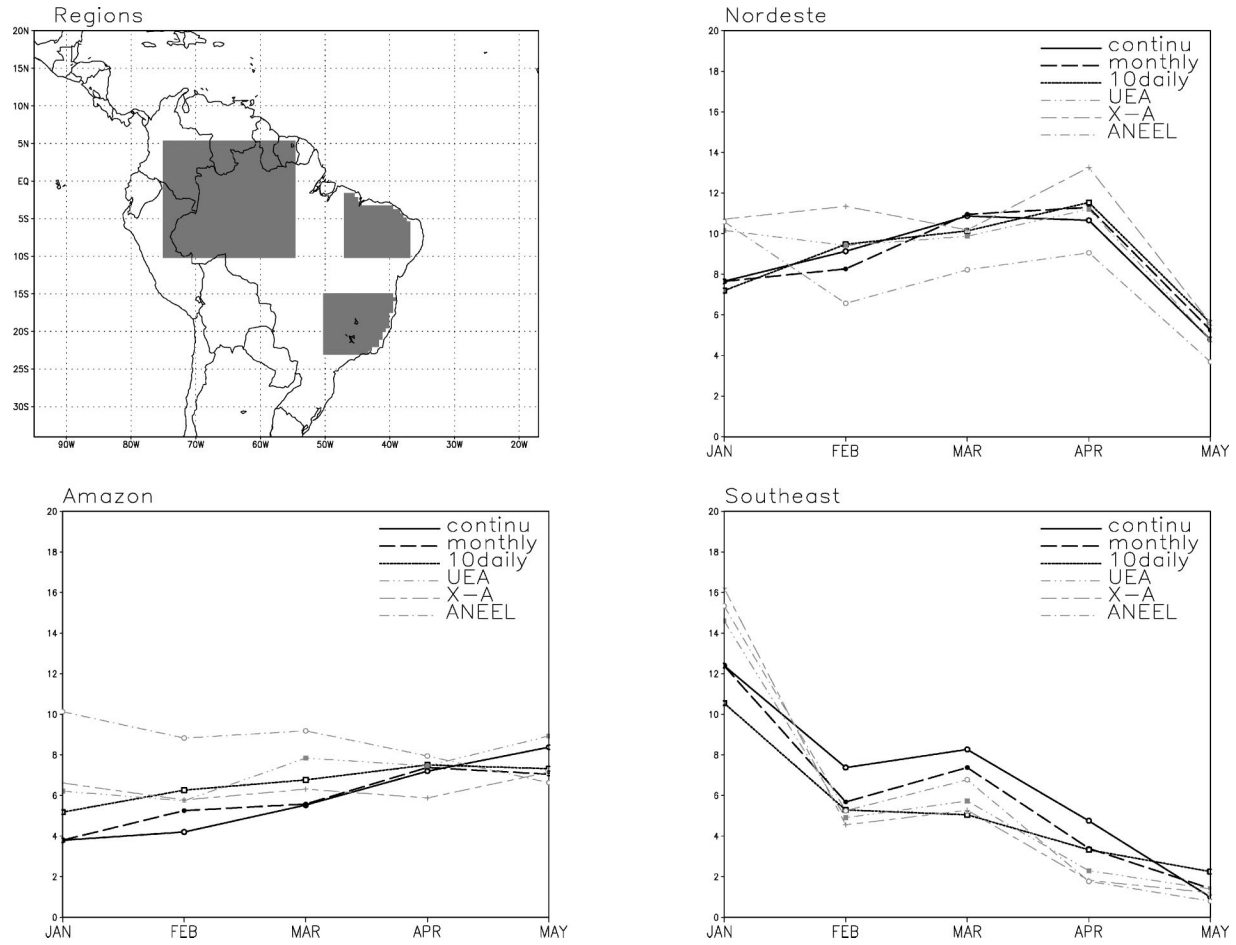

FIG. 3. Monthly precipitation (mm day^{-1}), Jan–May 1985. The six curves include three model simulations and three observations: 1) RegCM2 continuous run, 2) monthly reinitialized run, and 3) 10-day reinitialized run, 4) University of East Anglia (UEA), (5) Xie–Arkin (X–A), and (6) ANEEL stational observation.

sequent gradual adjustment on the timescale of about 2 weeks.

The first stage of adjustment is rapid. Unlike the unbounded global models, the regional models are driven by external forcing of either reanalysis or GCM outputs. The coarse-resolution driving fields are interpolated to the high-resolution regional model grids to prepare the initial and lateral boundary conditions, which inevitably introduces some errors at small spatial scales. The incompatibility between the driving field and the regional model dynamics, as well as the error resulting from the interpolation process, causes the model to adjust rapidly from the initial condition to a state intrinsic to the model internal dynamics, usually within 1 or 2 days (as an initial shock). This initial spinup process involves geostrophic and hydrostatic adjustments (Blumen 1976; Hoke and Anthes 1976; Daley 1981). Initialization schemes for weather forecasts were designed to solve this problem by removing the initial imbalance between the raw initial conditions and the model internal dynamics. It should be noted that this imbalance always exists in the lateral boundary condition datasets used in the buffer zone throughout the whole period of time integration. No attempt has been made to achieve balance for these lateral forcings. For long-term regional climate modeling, considering the lateral boundary conditions are frequently updated in the process of time integration, it is not practical to initialize all the lateral boundary conditions throughout the period of integration.

To measure the difference between two datasets A and B (either reanalysis or model output dataset), two variables are defined: the root-mean-square difference (RMSD) and the averaged difference or bias (BIAS). For a given variable V,

$$\mathrm{RMSD(AB)} = \left[\frac{1}{N}\sum_{i=1}^{N}(V_{Ai} - V_{Bi})^2\right]^{1/2}, \qquad (5)$$

$$\mathrm{BIAS(A - B)} = \frac{1}{N}\sum_{i=1}^{N}(V_{Ai} - V_{Bi}), \qquad (6)$$

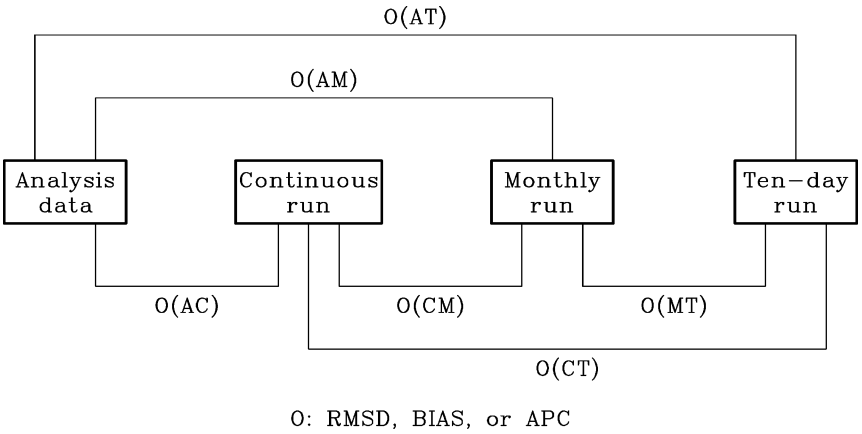

FIG. 4. Illustration of comparisons between four datasets: analysis data (A), continuous run (C), monthly reinitialized run (M), and 10-day reinitialized run (T). The operator O is either RMSD, BIAS, or APC, defined by Eqs. (5), (6), and (7), respectively.

where the summation is carried out over the number of grid points N within a given region. The RMSD reflects the averaged magnitude of deviation regardless of sign, while the BIAS measures predominant or systematic deviation in given directions. The calculations are among the following four datasets: analysis data (A), continuous run (C), monthly run (M), and 10-day run (T), as illustrated in Fig. 4. The operator O stands for either RMSD or BIAS, as defined above, or the anomaly pattern correlation (APC), to be defined in (7). For example, RMSD (AM) denotes the RMSD between the analysis and monthly runs, RSMD (AT) between the analysis and 10-day runs, and RSMD (MT) between the monthly and 10-day runs.

Figure 5 shows the evolution of RMSD (averaged over the whole domain D1) of some model variables from their corresponding reanalysis values in the first month of simulation (1–30 January). The RMSD between a transient state of model variables from their corresponding initial values (persistent, solid curve) are also shown as a reference for the range of the natural variability of each variable. Note that the monthly and continuous runs are identical in the first month of simulation (January). After starting the simulation from 0000 UTC 1 January 1985, the RMSD (AM) adjusted to a certain persistent level within about 2 days. An exception is that the surface pressure adjusted to its persistent level within 1 day, faster than the adjustment of the wind field. That implies that it is mostly the mass field adjusting to the wind field, thus the adjustment must occur at small spatial scales (i.e., much smaller than the Rossby deformation radius) according to the geostrophic adjustment theory. In order to avoid the inaccuracy caused by this kind of initial shock, all the 10-day and monthly reinitialized runs are actually started 2 days earlier, and the outputs of these first 2 days are not used for subsequent data analyses.

In their ''big brother'' experiment with a ''little brother'' domain of about 4500×4500 km^2 (which is smaller than our domain), Denis et al. (2002) also found that the little brother reproduced small-scale features in the lower and middle troposphere within about 1 day after the initial time (their Fig. 7). However, during this initial recovering or adjusting period, the precipitation in the little-brother experiment is much less than its virtual reality in the big-brother experiment (their Fig. 17), indicating that the precipitation, as a final product of the interactions of the dynamic and physical processes in the model, is very sensitive to the delicate physical imbalances among the adjusting variables.

Also reflected in Fig. 5 are the relative accuracies for the model to reproduce various fields. The RMSDs for P_s, T_{p200} (200-hPa temperature), $T_{\sigma.51}$ (air temperature on $\sigma = 0.51$), and all the zonal wind fields in lower, middle, and upper atmosphere ($u_{\sigma.895}$, $u_{\sigma.51}$, and u_{p200}, respectively) are notably smaller than the magnitudes of their persistent difference, indicating relatively high accuracy for these variables. However, the magnitudes of the RMSDs for $q_{\sigma.51}$ (specific humidity on $\sigma = 0.51$), $q_{\sigma.895}$ (specific humidity on $\sigma = 0.895$), and $T_{\sigma.895}$ (air temperature on $\sigma = 0.895$) are in the same level as their persistent RMSD, highlighting the low accuracy, hence the difficulties, in simulating the thermodynamics associated with the moisture processes in the lower atmosphere. Anthes et al. (1989), in their study of weather forecasting with a mesoscale model, also reported that the predictions of specific humidity are generally less skillful. In Fig. 5, it is also noticeable that the RMSD (MT) for $q_{\sigma.895}$, $T_{\sigma.895}$, and $u_{\sigma.895}$ are smaller than their RMSD (AM) and RMSD (AT) values, indicating that the model deviation from the reanalysis in the lower atmosphere is systematic, which will be discussed in more detail in section 6.

b. Subsequent slow adjustment

After the initial shock, the fields slowly approach the state of the continuous run as the second stage of tem-

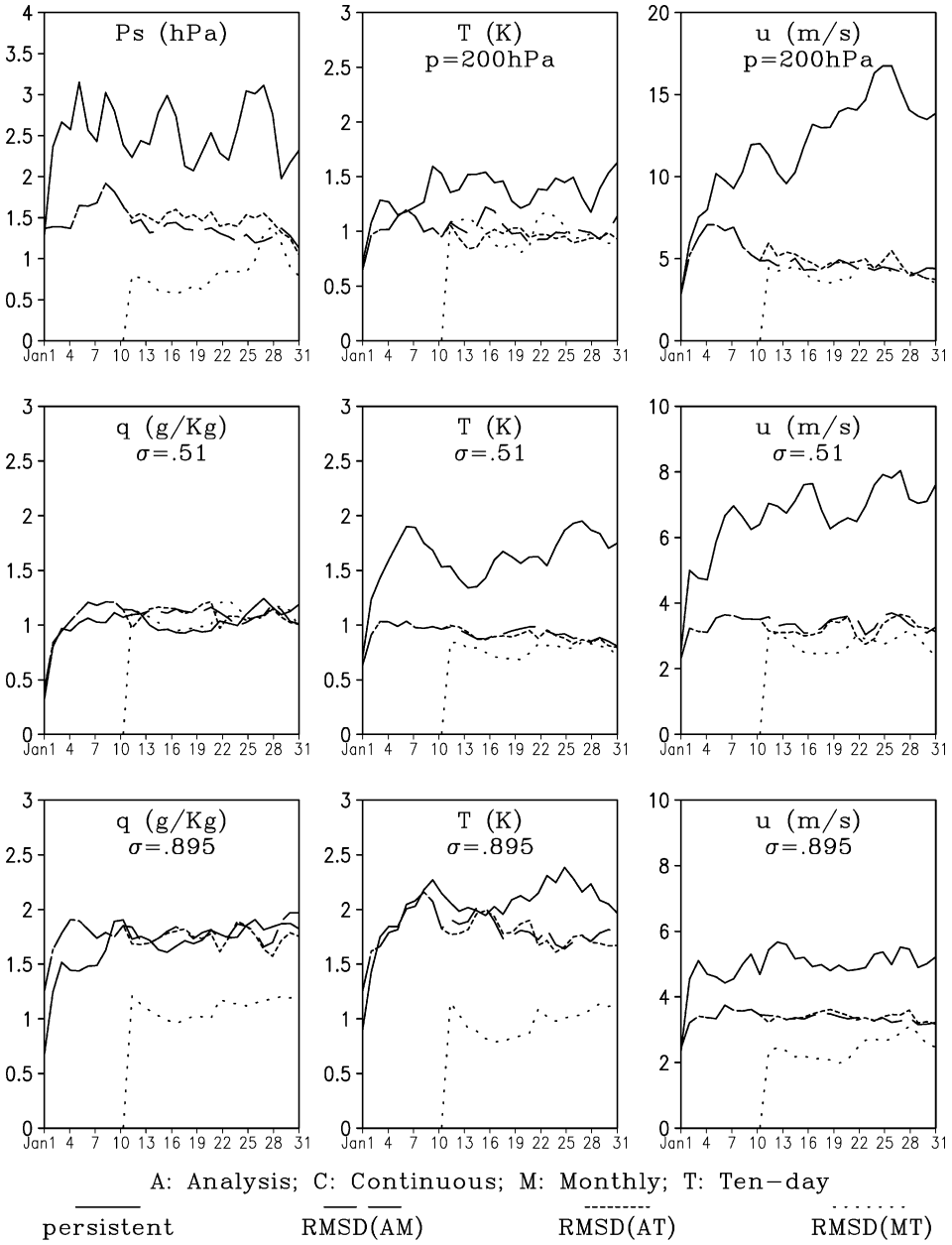

FIG. 5. Time series of the RMSD over the whole model domain for surface pressure P_s, specific humidity q at $\sigma = 0.51$ and 0.895, temperature T at $P = 200$ hPa and $\sigma = 0.51$ and 0.895, zonal velocity u at $p = 200$ hPa and $\sigma = 0.51$ and 0.895. The letters A, C, M, and T represent reanalysis, continuous run, monthly reinitialized run, and 10-day reinitialized run, respectively. RMSD(AM) is the RMSD between A and M. The solid curve (persistent) is the RMSD between the transient state of a variable and its value at 0000 UTC 1 Jan 1985.

poral adjustment. The time series of the biases (with respect to the analysis) of the various variables, averaged over the whole model domain, are plotted in Fig. 6. Since the monthly (long dash) and 10-day (short dash) runs are identical in the first 10 days of each month (or exactly each 30-day segment), the two curves overlap periodically. For the temperature at the 200-hPa surface (Fig. 6a), the continuous run has a systematic warm bias of about 1 K from the reanalysis values. The 10-day run periodically pulls the bias back to near zero. The state of each monthly run (long dash) adjusts to the continuous run (solid) in about 15 days. The bias evolves almost linearly with time in the first 15 days of each month in the monthly run, indicating that it is an increase of external or systematic error (Reynolds et al. 1994). In the lower atmosphere (Fig. 6b; $\sigma = 0.895$),

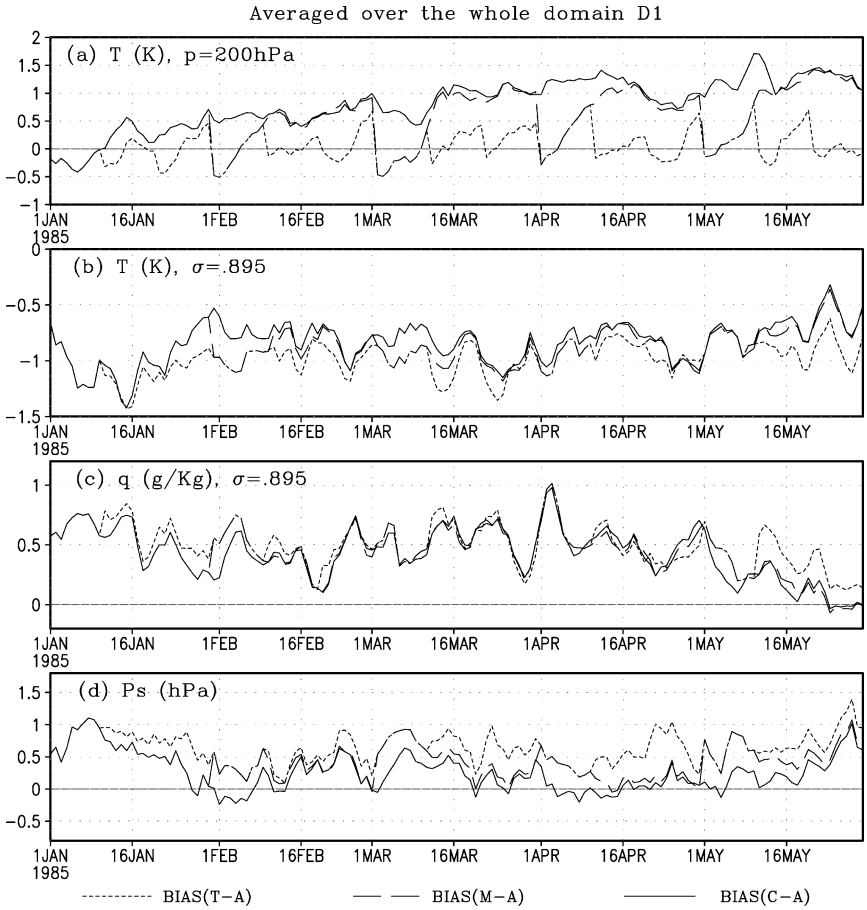

FIG. 6. Time series of area-averaged bias over the whole domain between a model run and the reanalysis. The solid, long-dashed, and short-dashed curves denote BIAS(C–A), BIAS(M–A), and BIAS(T–A) respectively, and A, C, M, and T represent reanalysis, continuous run, monthly reinitialized run and 10-day reinitialized run, respectively. Biases of T_{p200}, $T_{\sigma.895}$, $q_{\sigma.895}$, and P_s are in (a), (b), (c), and (d), respectively.

although all three model runs have a systematic cool bias of about -1 K, the magnitude of the fluctuation is smaller for the bias curve of the 10-day run. The temperature in the monthly run adjusts to that of the continuous run in about 15 days after the monthly reinitialization. For the low-level specific humidity at $\sigma = 0.895$ (Fig. 6c), the difference between the model runs are small, and there is a bias of between 0.0 and $+1.0$ g kg^{-1}. Therefore, the relative humidity in the lower atmosphere is higher in the model than in the reanalysis. To examine the mass conservation of the model, Fig. 6d shows the bias of the whole-domain-averaged surface pressure. For the continuous run, the initial positive bias decreases with time, indicating the achievement of balance between the total internal mass in the model domain and the fluxes through the lateral boundary. However, the model performance in precipitation has not benefited from the mass conservation in the continuous run; thus, the conservation must be accompanied by the distortion of other variables. The 10-day run always has larger positive mass bias than the continuous and monthly runs. Again, the bias of the monthly run asymptotes to the value of the continuous run in about 15 days after the reinitialization. The adjustment of T_{p200} is opposite to that of P_s in that the former adjusts from zero to a positive bias, while the latter adjusts from a positive bias to near zero, which is consistent because the colder air is heavier according to the hydrostatic relationship. Note that the trends of biases of the continuous run (as shown in Figs. 6a,d) do not necessarily reflect the long-term systematic trends in biases, but may simply reflect the seasonal cycle of model biases (Giorgi and Bi 2000).

Since the 10-day run generally performs better than the monthly and continuous runs in monthly rain rate, especially in the Amazon region, as shown in Fig. 3, the evolution of the biases to the corresponding reanalysis data is shown with the daily precipitation for further comparison (Fig. 7; 1 January–1 April, averaged in 10°S–5°N, 75°–55°W). The daily precipitation observation is available in the ANEEL data, which is shown by the thick dash–dot line in Fig. 7d. Although the ANEEL precipitation is larger than all the model-

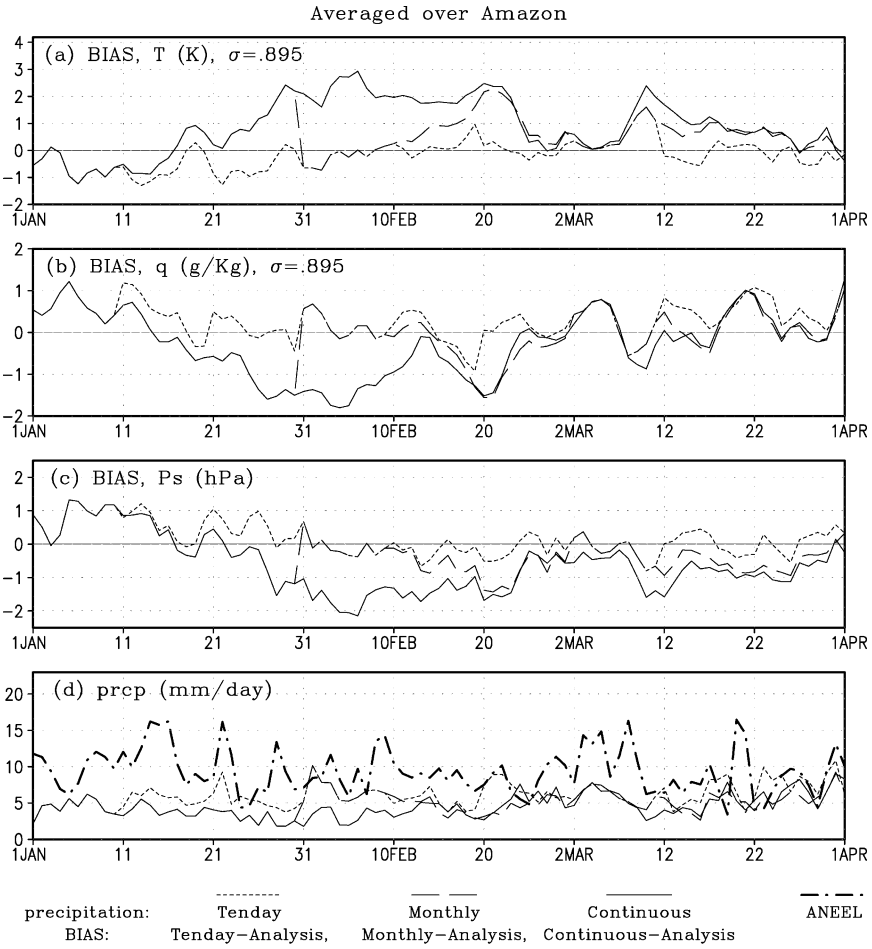

FIG. 7. Same as Fig. 6, but for the first 90 days and averaged over the Amazon basin instead of the whole domain. Note that plotted in (d) are not biases but precipitations of the 10-day reinitialized run (short dashed), monthly reinitialized run (long dashed), and continuous run (solid). Also shown in (d) is the observational ANEEL daily precipitation (thick dash–dot).

simulated precipitations, especially in the first 2 months, the 10-day run (short dash) is the closest to the observation. The rain rate of the monthly run (long dash) asymptotes to that of the continuous run (solid) in about 15 days after the reinitialization of each month. Considering that the ANEEL precipitation is also much larger than the UEA and XA data (as seen in Fig. 3), implying uncertainties in the validating observational data, the real difference between the model-simulated precipitation and its reality might not be so large. The model bias to reanalysis in $T_{\sigma.895}$, $q_{\sigma.895}$, and P_s is shown in Figs. 7a, 7b, and 7c, respectively. For $T_{\sigma.895}$, the curve of bias of the 10-day run is below that of monthly and continuous runs, similar to that in Fig. 6. The magnitude of variability in the time series of the biases for the 10-day run is also smaller than that for the continuous run. So the short-term runs keep the model from drifting too far away from the reanalysis data. The monthly run asymptotes to the continuous run in about 15–20 days after the reinitialization. For $q_{\sigma.895}$, the magnitude of fluctuation is also smaller in the 10-day run. For P_s, the initial positive bias in 1 January decreases with time to a negative equilibrium state, and the bias of the 10-day run fluctuates around zero. Note that the period of the maximum difference between the biases of the 10-day and continuous runs, which is roughly from the middle of January to the middle of Febuary, corresponds to the maximum difference of precipitations between the 10-day and continuous runs.

It is comprehensible that the timescale of the slow adjustment should depend on the domain size and geographical location of regional models. The bigger the domain is, the longer it takes for the model to reach an equilibrium. Moreover, if the domain is in the midlatitude where baroclinicity and the associated ''flushing'' effect of wind advection is stronger, the regional model simulation would be less sensitive to reinitialization. But in the Tropics, where the nature of the atmosphere is more convectively driving, the lateral boundary condition should be less important, and the model results

should be more sensitive to reinitialization. If the reinitialization of soil variables is also involved, then the timescale for the slow adjustment is also dependent on the mean climate and soil depth, as well as how the role of vegetation in evaporation is parameterized in the model (Scott et al. 1997; Xu et al. 1996). For example, the atmospheric response to soil wetness in the warmer Tropics is faster than that in the colder high latitude (Serafini 1990), and a model with a surface-vegetation-atmosphere-transfer scheme to account for vegetation evapotranspiration responds faster than a bucket land surface model without the vegetation-evapotranspiration capability (Scott et al. 1997).

5. Effects of lateral boundary forcing on the interior of the domain

The anomaly pattern correlations between different model runs or between reanalysis and model runs have been calculated to examine the effects of lateral forcing versus initial condition. The APC between the variable V of the two datasets A and B is defined as

$$\text{APC(AB)} = \frac{[V'_A V'_B]}{[(V'_A)^2]^{1/2}[(V'_B)^2]^{1/2}}, \qquad (7)$$

where V'_A and V'_B are the time anomalies of V_A and V_B, respectively. The brackets represent the spatial average over a certain domain. The APC measures how the spatial patterns of V_A and V_B in a given domain resemble each other at a particular time.

For each variable, APCs are calculated and averaged for each 10-day segment for the four domains, D1, D2, D3, and D4, shown in Fig. 1, with D1 the whole model domain, D2 the central part of D1 with the lateral buffer zone excluded, D3 one-fourth the area of D1, and D4 one-sixteenth the size of D1. The smallest domain is the farthest from the lateral boundary. The difference among the APCs of the four domains represents the degree of the domination by the lateral boundary forcing. Figure 8 shows the APCs for four variables, V_{p200}, $V_{\sigma.895}$ (wind speed on 200 hPa and $\sigma = 0.895$, respectively), $q_{\sigma.895}$, and P_s. (Recall that the reanalysis data and the continuous, monthly, and 10-day simulations are denoted by A, C, M, and T, respectively, and acronyms of APC for pairs of datasets are illustrated in Fig. 4.) The monthly run is somewhere between the continuous and 10-day runs, so that the curves of APC(AM) fall between APC(AC) and APC(AT), and those of APC(MT) fall between APC(CM) and APC(CT); hence, for clarity they are not shown. For the first 10 days in each month, the monthly run is identical to the 10-day run; therefore, APC(CM) is identical to APC(CT). In the second and third 10 days in each month, the monthly run becomes closer to the continuous run than to the 10-day run [i.e., for a given field, APC(CM) is larger than the corresponding APC(MT); not shown]. For the period of the very first 10 days (1–10 January), the 10-day run is identical to the continuous run; hence, APC(CT) = 1. Similarly, for the period of the first month (1–30 January), APC(CM) = 1.

The first point shown in Fig. 8 is that APC(AC) and APC(AT) (which are APCs between the analysis and model runs) are close to each other, and APC(CM) and APC(CT) (which are APCs between model runs) are close to each other. The closeness of the two curves of APC(AC) and APC(AT), on the one hand, demonstrates the stability of the internal dynamics and physics of RegCM2 for long-term climate simulations and, on the other hand, proves that the regional model is effectively controlled by the driving lateral boundary conditions. The dominant role of the lateral forcing keeps the model atmosphere from drifting away from the reanalysis, unlike the unbounded global models. Hence, the APCs between the simulation and reanalysis are not increased by the 10-day reinitializations [i.e., APC(AT) and APC(AC) have similar magnitude]. These comparisons indicate that even though the corruption by the errors from the lateral boundary (Errico et al. 1993; Warner et al. 1997; Qian et al. 1999) does not appear to cause serious stability problem in long-term continuous integration, the updating of initial condition makes a difference in the subtle precipitation processes, as shown in section 3. Moist convection onset is triggered by exceeding threshold values; therefore, small differences in model variables can give rise to large differences in precipitation rates.

Second, the magnitude of APC(AC) and APC(AT) is smaller than that of the corresponding APC(CM) and APC(CT) in the lower atmosphere ($V_{\sigma.895}$, $q_{\sigma.895}$, P_s), and this is also true in the middle atmosphere (not shown). However, in the upper atmosphere (V_{p200} as well as T_{p200}; the latter is not shown), the magnitude of APC(AC) and APC(AT) is close to that of APC(CM) and APC(CT). This implies that the difference between two model simulations is smaller than that between the reanalysis and a model simulation (i.e., model simulations are more alike to each other than to the reanalysis) in the middle and lower atmosphere. Takle et al. (1999) also reported that common tendencies exist even in the climate simulations by different regional models. The common feature in all the APCs between simulation and reanalysis indicates that the differences are systematic. Since the reanalysis is obtained by using observational data assimilation, the differences between the simulation and reanalysis presumably result from systematic errors in the model.

Also noted is that the APC values for surface pressure P_s, the mass variable, are higher than those of other fields in Fig. 8. The APCs of P_s also increase with time from the austral summer (January–Febuary) to fall (May), indicating better performance when temperature is cooler. These seasonal increases of APC are also found for $V_{\sigma.895}$ in D1 to D4 and for V_{p200} in D1 and D2. For humidity field $q_{\sigma.895}$, the value of APC(AT) is larger than that of APC(AC) in the last 2 months, and APC(AC) decreases with time in D4, indicating the ac-

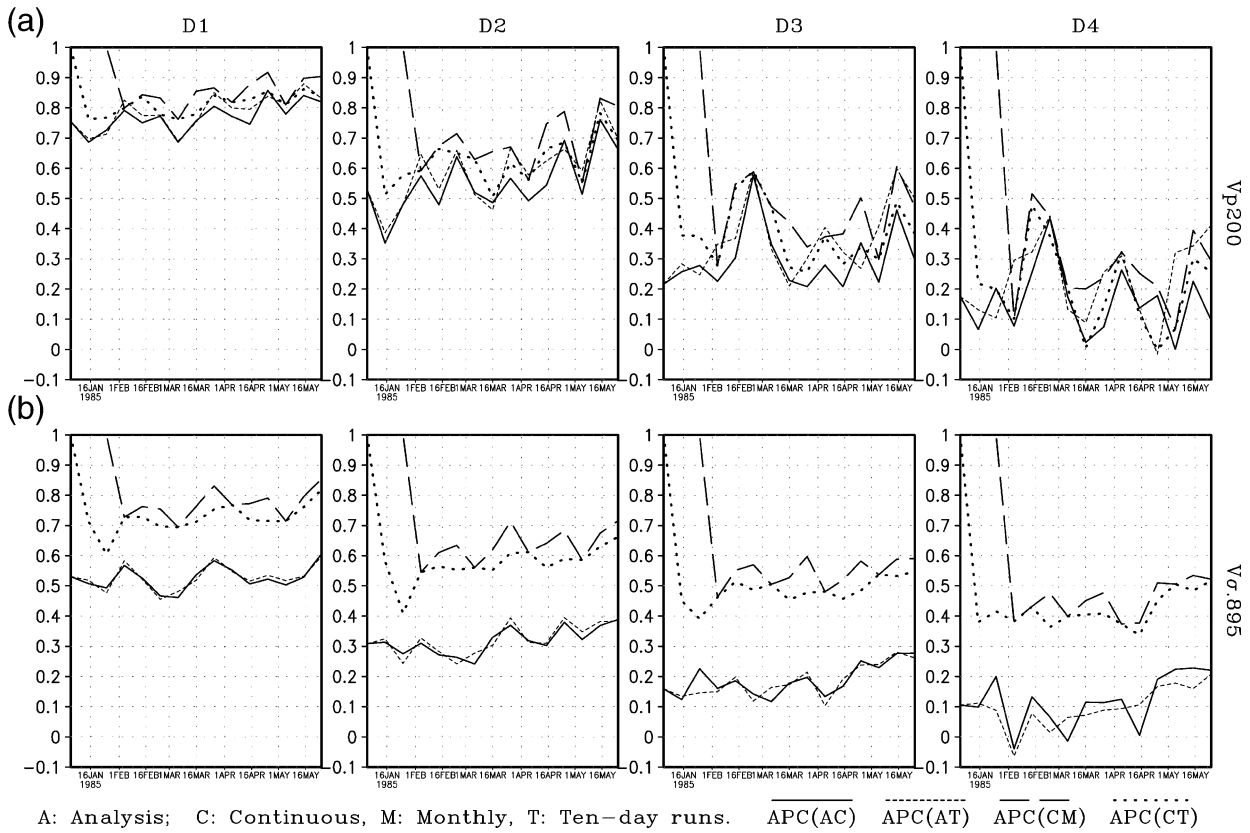

FIG. 8. Time series of the APC averaged over domain D1 to D4 (see Fig. 1) for various variables, between a model run and the reanalysis, or between different model runs. For example, APC(AC) is the APC between the reanalysis (A) and the continuous run (C). The APCs are calculated for the following variables: (a) V_{p200}, (b) $V_{\sigma.895}$ (wind speed at $P = 200$ hPa and $\sigma = 0.895$, respectively), (c) $q_{\sigma.895}$ (specific humidity at $\sigma = 0.895$), and (d) P_s (surface pressure).

cumulation of systematic errors in this field with the time of integration.

Lastly, the APCs decrease with the size of the domains, from D1 to D4. This indicates the weakening control of lateral boundary forcing for the domains away from the boundary. It may also be caused by the decreasing of deterministic predictability from large to small spatial scales in regional models, as shown by Laprise et al. (2000). To quantify, Table 1 lists the time-averaged values of APC(AT) and APC(CT) for the four domains, representing the APC between a model simulation and the reanalysis and the APC between two simulations, respectively. For example, for T_{p200}, the time-averaged APC(AT) is 0.59, 0.29, 0.22, and 0.25 for D1 to D4, respectively. All the APCs are positive, even in the smallest domain, D4. However, the APCs are rather small for D4. Comparing APCs of $T_{\sigma.51}$ and $T_{\sigma.895}$, their corresponding values of APC(AT) are of similar magnitude, but APC(CT) for $T_{\sigma.895}$ is larger than the corresponding values of APC(CT) for $T_{\sigma.51}$ (i.e., the model runs are more alike at $\sigma = 0.895$), indicating that differences made by the model are more systematic in the lower atmosphere. Similar features are found in the specific humidity fields $q_{\sigma.51}$ and $q_{\sigma.895}$; that is, APC(CT) is larger in the lower atmosphere. For P_s and the surface temperature T_s, the APCs, especially APC(CT), are quite large for all domains, indicating the well-preserved bulk effect in surface variables by the regional model despite the artificial tuning and possible distortions in the physics parameterization schemes. For the wind speed fields (V), APCs in the upper atmosphere (V_{p200}) are larger than the corresponding values in the lower atmosphere ($V_{\sigma.895}$), indicating a stronger ''flushing'' mechanism by the lateral boundary forcing in the upper atmosphere (McGregor 1997). The exceptions are the APC(CT) of wind fields in D3 and D4, in which lower levels have larger values, indicating enhanced similarities in mesoscale circulations between different model runs, owing to the orientation by the high-resolution bottom topography.

6. Systematic errors

The systematic errors in a regional climate model result from either the large-scale driving fields or the regional model physics itself (Noguer et al. 1998). Since the reanalysis is used as the driving field in the current study and is taken as the basis to make comparison with,

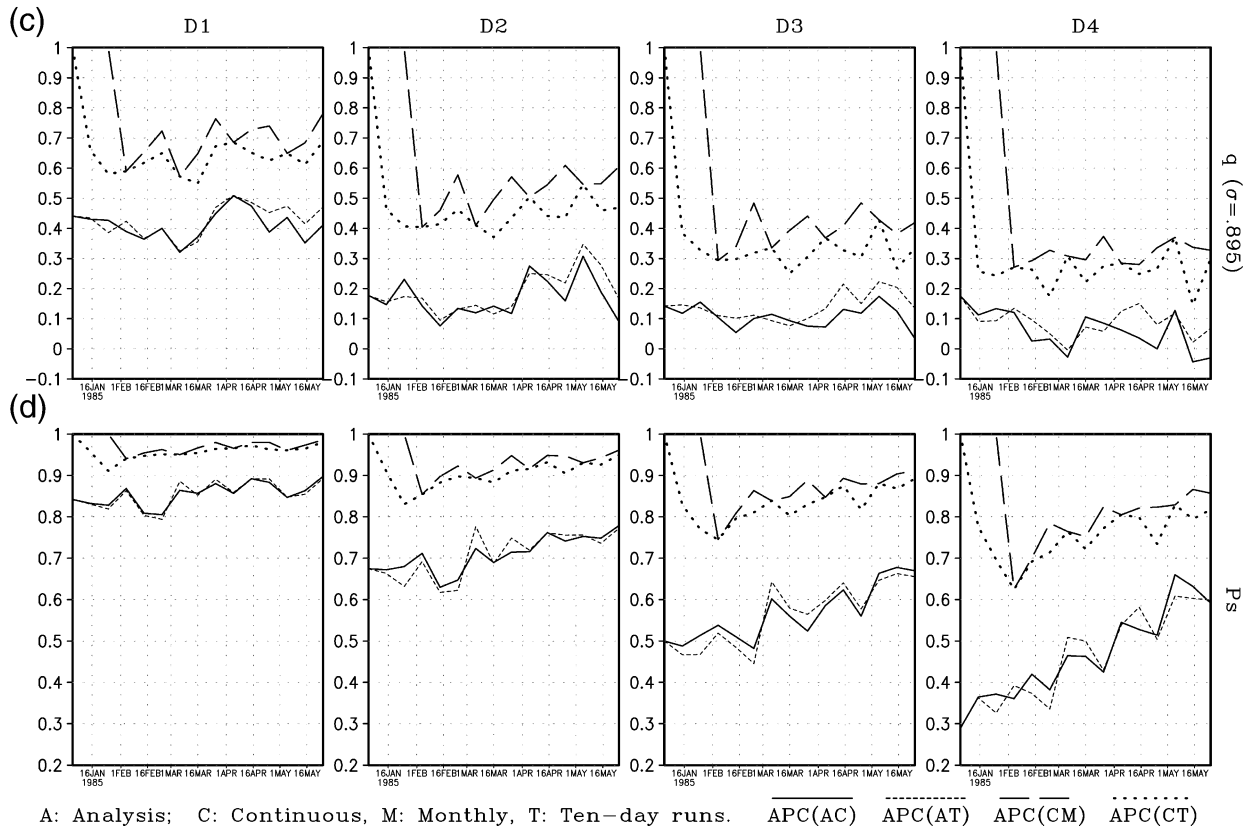

FIG. 8. (*Continued*)

the errors discussed below are from the deficiency in the regional model physics. To discern the systematic drift from the effect of internal variability of regional models (Giorgi and Bi 2000; Christensen et al. 2001), the 5-month averaged biases are calculated for several variables along two latitudes and shown with corresponding topographies and land–sea masks.

The biases of various variables between model run and reanalysis (C–A, M–A, and T–A) along the equator are shown in Fig. 9. The Andes, with a peak of about 1.6 km, are between 75° and 80°W, and the Amazon mouth is roughly at 50°W. The two vertical thin long dash lines shows the positions of the inner boundaries of the lateral buffer zones. The biases are zero at the outer lateral boundaries where the model variables are taken as their reanalysis values. Because the relaxation coefficient is exponential in the buffer zone diminishing inward, the strong stipulation of the reanalysis is limited within several grids to the outer lateral boundary. For the temperature fields, the diversity among the three bias curves (which also reflects the differences among the three model runs) is larger in upper atmosphere (200 hPa) than in the middle and lower atmosphere (σ = 0.51, 0.895, respectively). For T_{p200}, BIAS (T–A) (the time-averaged bias between 10-day run and reanalysis) is smaller than BIAS (C–A), and the bias over land is smaller than that over the Atlantic Ocean. The effect of the Andes Mountains appears weak in the upper atmosphere. In the middle atmosphere, the biases of $T_{\sigma.51}$ show that the differences between the three runs are small, with the 10-day run being slightly closer to the reanalysis (i.e., the absolute value of the bias is smaller). However, the Andes Mountains have a notable effect, impinging a negative bias of over 1 K east of the peak with decreased magnitude eastward. The bias over the ocean is also negative, unlike that of T_{p200}. The specific humidity $q_{\sigma.51}$ has a positive bias over the land, with a

TABLE 1. Time-averaged values of APC. Here A is the reanalysis, C is the continuous run, and T is the 10-day initialized run.

	APC(AT)				APC(CT)			
	D1	D2	D3	D4	D1	D2	D3	D4
T_{p200}	0.59	0.29	0.22	0.25	0.62	0.39	0.32	0.31
$T_{\sigma.51}$	0.70	0.41	0.19	0.10	0.76	0.55	0.34	0.25
$T_{\sigma.895}$	0.64	0.40	0.30	0.06	0.80	0.65	0.54	0.39
T_s	0.69	0.61	0.65	0.58	0.86	0.81	0.79	0.71
P_s	0.85	0.71	0.56	0.46	0.96	0.91	0.84	0.77
$q_{\sigma.51}$	0.39	0.22	0.13	0.07	0.44	0.33	0.26	0.22
$q_{\sigma.895}$	0.43	0.19	0.14	0.09	0.65	0.48	0.37	0.31
V_{p200}	0.79	0.59	0.36	0.23	0.82	0.65	0.42	0.25
$V_{\sigma.51}$	0.67	0.43	0.27	0.20	0.76	0.58	0.44	0.38
$V_{\sigma.895}$	0.53	0.32	0.18	0.10	0.74	0.60	0.52	0.46

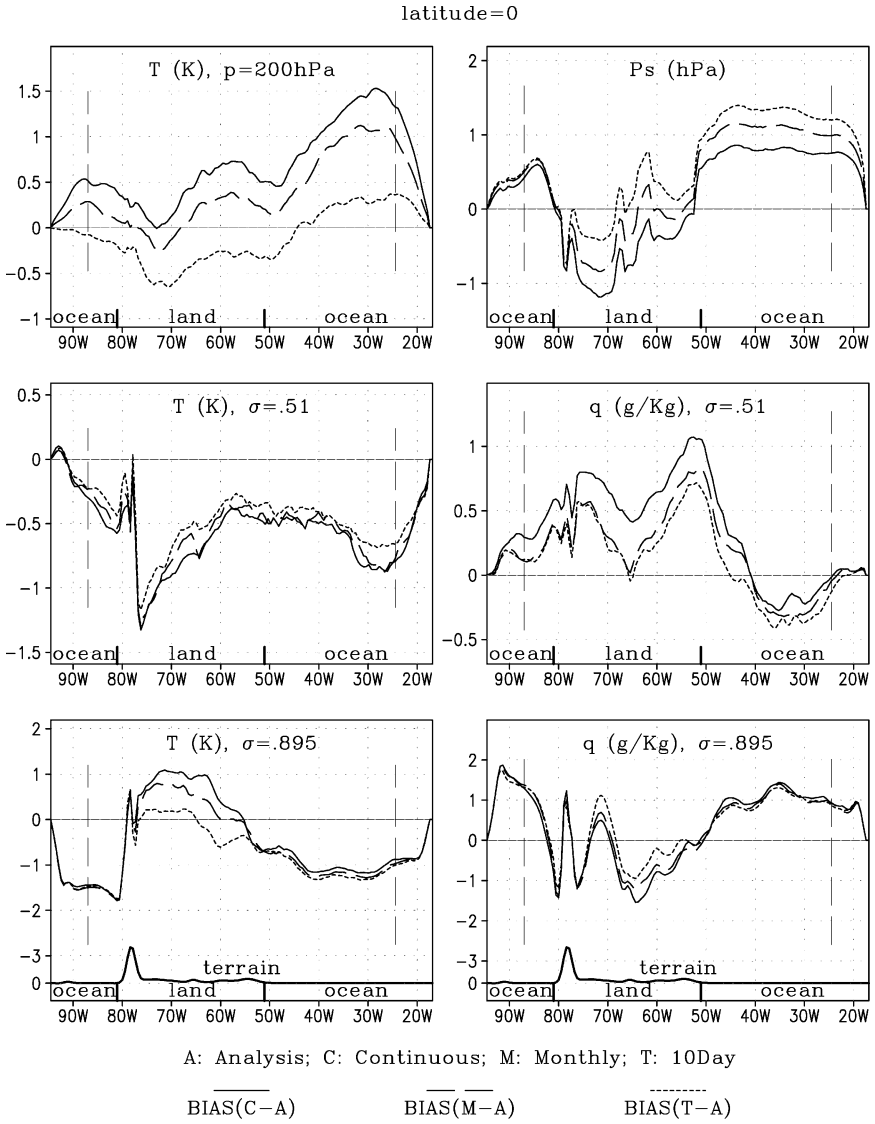

FIG. 9. The 5-month averaged bias of T_{p200}, $T_{\sigma.51}$, $T_{\sigma.895}$, P_s, $q_{\sigma.51}$, and $q_{\sigma.895}$ between model simulation and reanalysis along the equator. Also shown are the terrain and land–sea masks.

maximum over the east coast, but a negative bias over the Atlantic. Again, the $q_{\sigma.51}$ in the 10-day run is the closest to its corresponding reanalysis values. In the lower atmosphere, the bias of $T_{\sigma.895}$ is positive over land, with BIAS (T–A) being the smallest. This increase of low-level temperature coincides the underestimation of precipitation over the Amazon basin. Over the ocean, the temperatures in the three runs are very close to each other, and the negative biases are over 1 K in both the Pacific and the Atlantic. But the specific humidity $q_{\sigma.895}$ has a positive bias over the oceans, so the temperature and moisture fields in the marine atmospheric boundary layer both favor more precipitation over the ocean. Fluctuation of bias curves of $q_{\sigma.895}$ are over the land east of the Andes. In the surface pressure field, the biases of P_s are positive over the ocean, with a magnitude of about 1 hPa in all three runs, but negative over the land in the monthly and continuous runs. Gyakum et al. (1996) also found these kinds of systematic errors in a regional model intercomparison experiment of oceanic cyclogenesis forecasting. The value of BIAS(T–A) of P_s is close to zero in the equatorial Amazon basin between 60° and 70°W, corresponding to the best simulation of Amazon precipitation by the 10-day run among the three simulations. Over the Atlantic, however, the BIAS(T–A) of P_s is larger than BIAS(C–A), with the larger positive bias of P_s corresponding to the smaller bias of T_{p200}. A sharp spatial variation of the biases of P_s is at the east coast, with the small bias over the land and an abrupt increase to the ocean. The surface pressure is

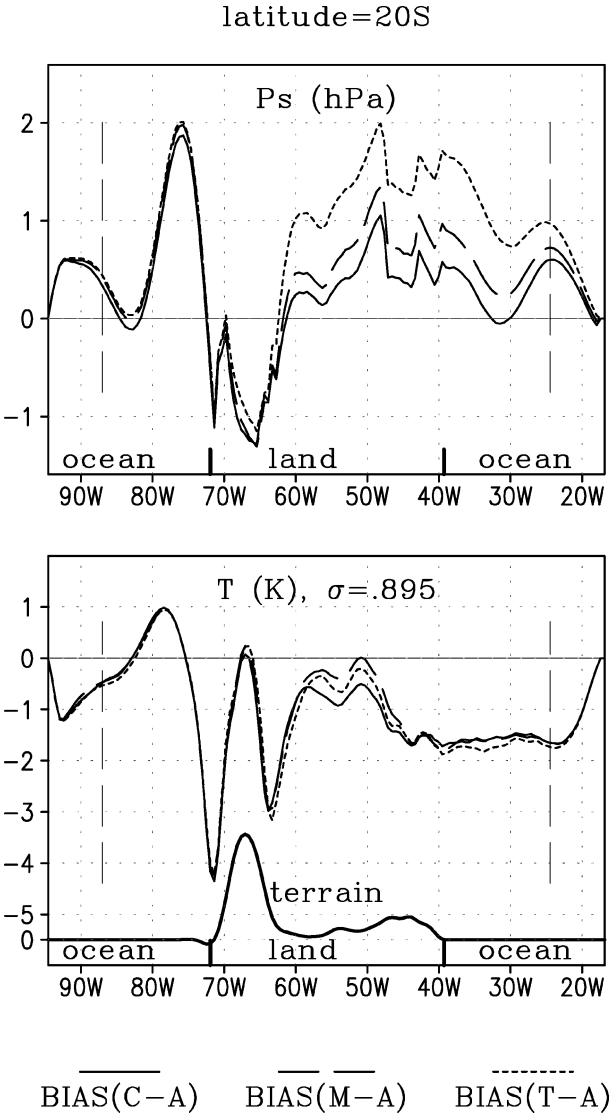

FIG. 10. Same as Fig. 9, but for P_s and $T_{\sigma.895}$ along the latitude of 20°S.

systematically increased by the model over the oceans, which imposes a pressure gradient along the east coast, fostering excessive coastal precipitation.

Along the latitude of 20°S (Fig. 10), the peak of the Andes is at about 67°W, and the South American continent crosses from about 72° to 39°W, with oceans to the west and east. The height of the peak of the Andes is about 4.5 km in the model, much higher than that at the equator. Therefore, a much stronger effect of the Andes on the atmosphere can be seen in the biases between the regional model simulation and the reanalysis data. The biases, to some extent, represent the high-resolution correction of the coarse-resolution reanalysis data. On the other hand, the systematic errors from regional model deficiencies also result in large biases. Since the high-resolution observational data over the Andes are rare and unavailable for validation, it is difficult to exactly delineate the numerical error caused by the steep Andes Mountains. In Fig. 10, the 5-month averaged bias of $T_{\sigma.895}$ is as large as −4 K at the west side of the Andes, and the bias of P_s is as large as 2 hPa near the Pacific coast. These large biases near the Andes indicate the existence of model systematic errors associated with the high and steep mountains. The relative differences among the three bias curves near the Andes are rather small, implying that the systematic error resulted from the steep mountain's rapidly reaching a persistent level and not changing much afterward. However, the existence of the large persistent error over the Andes could contaminate the simulation in other places, particularly downstream, through advection and other nonlinear interactions. In contrast, the differences among the three bias curves are relatively large over the ocean and land areas away from the Andes Mountains, indicating the slow accumulation of systematic errors from other deficiencies in the surface and atmospheric processes of the model. The application of reinitialization helps to mitigate the effect of the accumulation and contamination of these systematic errors.

Above analyses reveal that major systematic errors of the model exist near the Andes and over the oceans. The contrast between land and ocean is also clear. The numerical representation of physical processes near the ''knife edged'' Andes, such as the calculation of the pressure gradient force, could possibly cause large errors and generate gravity waves affecting other areas. The large RMSD value in the low-level temperature and humidity fields also points to the model deficiencies in the tropical marine atmospheric boundary layer.

It is also evident in Figs. 9 and 10 that the differences among the three bias curves are generally smaller than the magnitude of the bias (a measure of systematic error). Therefore, even though the 10-day run gives the best result, it is still generally close to the other model runs and less close to the observation and reanalysis, implying that all model simulations suffer from the same source of systematic errors. Therefore, fundamental improvements in downscaling accuracy should still rely on model improvements to dynamical structures (such as the pressure gradient scheme near steep topography) and physics parameterization schemes (such as marine boundary layer and cumulus parameterizations) to reduce systematic errors. But considering the practical issue that all numerical models are imperfect, at least when using analyses of observations to produce lateral boundary fields, the strategy of reinitialization provides an expedient way of minimizing these numerical and physical limitations based on currently available tools, so as to mitigate the effect of internal (nonlinear) and external (systematic) error growth.

7. Summary and discussion

By using a regional climate model RegCM2, we compare the long-term continuous integration with consec-

utive medium- and short-term reinitialized simulations to study their relative performance and error growth in the practice of dynamic downscaling. Compared to the observed precipitations, the 10-day reinitialized run results in the smallest error among the three model simulations, and the continuous run shows larger error. The temporal adjustment from the reanalysis to the model equilibrium state experiences two stages. In the first 1 or 2 days, it is rapidly adjusted to a state intrinsic to the model dynamics, in the process of removing small-scale imbalances through geostrophic adjustments from mass to wind field. In the subsequent second stage, in the timescale of about 15–20 days, the model variables gradually adjust to a state close to that of the long-term continuous run. After this, the monthly runs are almost identical to the continuous run, indicating that a balance has been reached between the lateral forcing and the regional model dynamics. This kind of temporal evolution and their relative performance reveal that the model error gradually increases with time for about 15 days, until an equilibrium stage is reached that seemingly has extended predictability. The above results support the idea of consecutive short-term reinitialized runs for regional climate downscaling when analyses of observations are used for lateral boundary conditions. As pointed out by Pan et al. (1999), another advantage of this approach is the ability to run the model over different periods in parallel.

Denis et al. (2002) studied the accuracy of regional climate models in reproducing precipitation. The time series of the area-averaged precipitation rates (their Fig. 17) showed poor accuracy in the initial shock period of the first 1 or 2 days, very high accuracy from about day 2 to day 12, and then degraded accuracy after day 13, possibly due to accumulation of systematic errors. Their finding is consistent with that from the present study, suggesting the advantage of the strategy of the 10-day reinitialized run for downscaling, that is, a sequence of 12-day reinitialized runs, with the outputs of the first 2 days discarded.

The results also show that all the model runs are similar, but rather different from the reanalysis. On the one hand, it demonstrates the manipulating role of lateral boundary forcing to the regional model. On the other hand, it indicates the common sources of errors in different model runs. Compared to unbounded global models, the internal variability is restrained in regional models because of the control of lateral boundary conditions. The test of physics parameterization schemes, however, might benefit from this restraint in regional models because the response to a parameter could be singled out without being complicated by free global interactions. The APCs over D1 to D4 show the decreased pattern correlation when the diagnosis domain is moved farther away from the lateral boundary. Therefore, the center of the domain is subject to weaker control from lateral forcing.

If the desired area for the downscaling is far away from the lateral boundary, the nudging method might be desirable to provide more reliable large-scale forcing inside the area of interest to prevent the regional models from drifting away from its large-scale driving fields. Kida et al. (1991) and Sasaki et al. (1995) proposed a spectral nudging method for a regional climate model, in which the low-wavenumber spectral components (corresponding to large-scale conditions) in the regional model were replaced periodically by its counterparts in the large-scale driving fields (reanalysis or GCM outputs). Without the spectral nudging, their simulated synoptic circulation (such as cyclones and anticyclones) was distorted compared to the driving field after about a week. And a remedy was found by applying the spectral nudging every 12 h. Von Storch et al. (2000) also demonstrated that the spectral nudging method was successful in keeping the simulated states close to the driving state at large scales, while generating small-scale features. However, caution also needs to be taken when using the nudging method because cases exist in which the regional model improves the synoptic-scale features that are not presented in the driving GCM fields. For example, Giorgi et al. (1990) showed cases of Alpine lee cyclones simulated by a nested regional climate model that were not present in the driving GCM; Giorgi et al. (1998) improved precipitation over the central United States by using a nested regional climate model with a better representation of the Rockies. In these cases, the spectral nudging would have prevented substantial improvement.

It should be pointed out that the current downscaling study is based on the reanalysis-driving mode, in which the driving field is assumed to be perfect. If the driving fields are derived from an imperfect GCM prediction rather than the analyses of observations, then the regional model is subject to the effect of the two potentially contradictory factors: one is the improvement induced by the high-resolution dynamics and physics of the regional model, and the other is the possible adverse effect of the accumulation of systematic errors resulting from the long-term continuous integration of the regional model. In the GCM-driving case, similar fast adjustment (initial shock in the timescale of 1 to 2 days) to that discussed in section 4a would still occur, after which the regional model would have produced high-resolution features associated with the better-resolved topography and local forcing in the regional model. Of course, the downscaling performance first depends on the quality of those high-resolution features (absent in GCMs). Second, it is also affected by the error growth rate in the slow adjustment period (in the timescale of 2 weeks or longer) that is associated with the accumulation of systematic errors. Further studies of reinitialization of regional climate models in the GCM-driving mode is warranted.

Acknowledgments. We wish to thank Dr. Filippo Giorgi, the developer of RegCM2. This study was supported

by the NOAA Application Research Centers (ARCs) project. Computation was provided by the NCAR CSL project. The International Research Institute for Climate Prediction represents a cooperative agreement between the NOAA Office of Global Programs and Columbia University.

REFERENCES

Anthes, R. A., Y.-H. Kuo, D. P. Baumhefner, R. M. Errico, and T. W. Bettge, 1985: Predictability of mesoscale motions. *Advances in Geophysics*, Vol. 28, Academic Press, 159–202.

——, ——, E.-Y. Hsie, S. Low-Nam, and T. W. Bettge, 1989: Estimation of skill and uncertainty in regional numerical models. *Quart. J. Roy. Meteor. Soc.*, **115,** 763–806.

Blumen, W., 1976: Experiments in atmospheric predictability: Part I. Initialization. *J. Atmos. Sci.*, **33,** 161–169.

Christensen, O. B., M. A. Gaertner, J. A. Prego, and J. Polcher, 2001: Internal variability of regional climate models. *Climate Dyn.*, **17,** 875–887.

Daley, R., 1981: Predictability experiments with a baroclinic model. *Atmos.–Ocean*, **19,** 77–89.

Denis, B., R. Laprise, D. Caya, and J. Cote, 2002: Downscaling ability of one-way nested regional climate models: The big-brother experiment. *Climate Dyn.*, **18,** 627–646.

Dickinson, R. E., R. M. Errico, F. Giorgi, and G. T. Bates, 1989: A regional climate model for the western United States. *Climatic Change*, **15,** 383–422.

——, A. Henderson-Sellers, and P. J. Kennedy, 1993: Biosphere atmosphere transfer scheme (BATS) version le as coupled to the NCAR community climate model. NCAR Tech. Note, NCAR/TN-387+STR, 72 pp.

Druyan, L. M., M. B. Fulakeza, P. Lonegan, and M. Saloum, 2001: A regional model study of synoptic features over West Africa. *Mon. Wea. Rev.*, **129,** 1564–1577.

Errico, R. M., T. Vukicevic, and K. Reader, 1993: Comparison of initial and lateral boundary condition sensitivity for a limited-area model. *Tellus*, **45A,** 539–557.

Giorgi, F., and G. T. Bates, 1989: The climatological skill of a regional model over complex terrain. *Mon. Wea. Rev.*, **117,** 2325–2347.

——, and M. R. Marinucci, 1996: An investigation of the sensitivity of simulated precipitation to model resolution and its implications for climate studies. *Mon. Wea. Rev.*, **124,** 148–166.

——, and L. O. Mearns, 1999: Introduction to special section: Regional climate modeling revisited. *J. Geophys. Res.*, **104** (D6), 6335–6352.

——, and X. Bi, 2000: A study of internal variability of a regional climate model. *J. Geophys. Res.*, **105,** 29 503–29 521.

——, M. R. Marinucci, and G. Visconti, 1990: Use of a limited-area model nested in a general circulation model for regional climate simulation over Europe. *J. Geophys. Res.*, **95,** 18 413–18 431.

——, ——, and G. T. Bates, 1993a: Development of a second-generation regional climate model (RegCM2). Part I: Boundary layer and radiative transfer processes. *Mon. Wea. Rev.*, **121,** 2794–2813.

——, ——, and ——, 1993b: Development of a second-generation regional climate model (RegCM2). Part II: Convective processes and assimilation of lateral boundary conditions. *Mon. Wea. Rev.*, **121,** 2814–2832.

——, L. O. Mearns, C. Shields, and L. McDaniel, 1998: Regional nested model simulations of present day and 2 × CO_2 climate over the central plains of the U.S. *Climatic Change*, **40,** 457–493.

Grell, G. A., 1993: Prognostic evaluation of assumptions used by cumulus parameterizations. *Mon. Wea. Rev.*, **121,** 764–787.

Gyakum, J. R., and Coauthors, 1996: A regional model intercomparison using a case of explosive oceanic cyclogenesis. *Wea. Forecasting*, **11,** 521–543.

Hoke, J. E., and R. A. Anthes, 1976: The initialization of numerical models by a dynamic-initialization technique. *Mon. Wea. Rev.*, **104,** 1551–1556.

Holtslag, A. A. M., E. I. F. de Bruijn, and H.-L. Pan, 1990: A high-resolution air mass transformation model for short-range weather forecasting. *Mon. Wea. Rev.*, **118,** 1561–1575.

Horel, J. D., J. B. Pechmann, A. N. Hahmann, and J. E. Geisler, 1994: Simulations of the Amazon Basin circulation with a regional model. *J. Climate*, **7,** 56–71.

Ji, Y., and A. D. Vernekar, 1997: Simulation of the Asian summer monsoons of 1987 and 1988 with a regional model nested in a global GCM. *J. Climate*, **10,** 1965–1979.

Kida, H., T. Koide, H. Sasaki, and M. Chiba, 1991: A new approach for coupling a limited area model to a GCM for regional climate simulations. *J. Meteor. Soc. Japan*, **69,** 723–728.

Kiehl, J. T., J. J. Hack, G. B. Bonan, B. A. Boville, B. P. Briegleb, D. L. Williamson, and P. J. Rasch, 1996: Description of the NCAR Community Climate Model (CCM3). NCAR Tech. Note NCAR/TN-420+STR, 152 pp.

Laprise, R., M. R. Varma, B. Denis, D. Caya, and I. Zawadzki, 2000: Predictability of a nested limited-area model. *Mon. Wea. Rev.*, **128,** 4149–4154.

Lorenz, E. N., 1963: Deterministic nonperiodic flow. *J. Atmos. Sci.*, **20,** 130–141.

——, 1969: Atmospheric predictability as revealed by naturally occurring analogues. *J. Atmos. Sci.*, **26,** 636–646.

McGregor, J. L., 1997: Regional climate modelling. *Meteor. Atmos. Phys.*, **63,** 105–117.

Mo, K. C., and X. L. Wang, 1995: Sensitivity of the systematic error of extended range forecasts to sea surface temperature anomalies. *J. Climate*, **8,** 1533–1543.

New, M. G., M. Hulme, and P. D. Jones, 2000: Representing twentieth-century space–time climate variability. Part II: Development of 1901–96 monthly grids of terrestrial surface climate. *J. Climate*, **13,** 2217–2238.

Noguer, M., R. Jones, and J. Murphy, 1998: Sources of systematic errors in the climatology of a regional climate model over Europe. *Climate Dyn.*, **14,** 691–712.

Pan, Z., E. Takle, W. Gutowski, and R. Turner, 1999: Long simulation of regional climate as a sequence of short segments. *Mon. Wea. Rev.*, **127,** 308–321.

Pielke, R. A., Sr., 1998: Climate prediction as an initial value problem. *Bull. Amer. Meteor. Soc.*, **79,** 2743–2746.

Qian, J.-H., F. Giorgi, and M. S. Fox-Rabinovitz, 1999: Regional stretched grid generation and its application to the NCAR RegCM. *J. Geophys. Res.*, **104,** 6501–6513.

Reynolds, C. A., P. J. Webster, and E. Kalnay, 1994: Random error growth in NMC's global forecasts. *Mon. Wea. Rev.*, **122,** 1281–1305.

Sasaki, H., H. Kida, T. Koide, and M. Chiba, 1995: The performance of long-term integrations of a limited area model with the spectral boundary coupling method. *J. Meteor. Soc. Japan*, **73,** 165–181.

Scott, R., D. Entekhabi, R. Koster, and M. Suarez, 1997: Timescales of land surface evapotranspiration response. *J. Climate*, **10,** 559–566.

Serafini, Y. V., 1990: The time scale of land surface hydrology in response to initial soil moisture anomalies: A case study. *Tellus*, **42A,** 390–400.

Seth, A., and M. Rojas, 2003: Simulation and sensitivity in a nested modeling system for tropical South America. Part I: Reanalyses boundary forcing. *J. Climate*, **16,** 2437–2453.

Takle, E. S., and Coauthors, 1999: Project to intercompare regional climate simulations (PIRCS): Description and initial results. *J. Geophys. Res.*, **104,** 19 443–19 461.

von Storch, H., H. Langenberg, and F. Feser, 2000: A spectral nudging technique for dynamical downscaling purposes. *Mon. Wea. Rev.*, **128,** 3664–3673.

Warner, T. T., R. A. Peterson, and R. E. Treadon, 1997: A tutorial on lateral boundary conditions as a basic and potentially serious

limitation to regional numerical weather prediction. *Bull. Amer. Meteor. Soc.*, **78,** 2599–2617.

Wilby, R. L., 1997: Non-stationarity in daily precipitation series: Implications for GCM down-scaling using atmospheric circulation indices. *Int. J. Climatol.*, **17,** 439–454.

Xie, P., and P. A. Arkin, 1996: Analysis of global monthly precipitation using gauge observations, satellite estimates, and numerical model predictions. *J. Climate*, **9,** 840–858.

Xu, L., S. Raman, R. V. Madala, and R. Hodur, 1996: A non-hydrostatic modeling study of surface effects on mesoscale convection induced by sea breeze circulation. *Meteor. Atmos. Phys.*, **58,** 103–122.